

Systematic analysis of the decay of $^{287,288,290,292}\text{Fl}^*$ formed in the complete fusion reactions $^{239,240,242,244}\text{Pu} + ^{48}\text{Ca}$ including Skyrme forces

Nirupama Kumari,¹ Aman Deep,¹ Sahila Chopra,² and Rajesh Kharab¹

¹*Department of Physics, Kurukshetra University, Kurukshetra - 136119, India*

²*Frankfurt Institute for Advanced Studies (FIAS), Ruth-Moufang-Straße 1, 60438 Frankfurt am Main, Germany*



(Received 6 December 2022; accepted 23 December 2022; published 17 January 2023)

The fusion evaporation residue cross sections for the decay of the compound nuclear system $^{287,288,290,292}\text{Fl}^*$ via $2n$ - to $5n$ -decay channels, synthesized in $^{239,240,242,244}\text{Pu} + ^{48}\text{Ca}$, are studied using the dynamical cluster-decay model (DCM), including quadrupole deformations β_{2i} for compact hot orientations θ_i at various excitation energies $E^* = 32.5$ to 52.6 MeV. For the nucleus-nucleus interaction potentials, we have employed the Skyrme energy density functional based on the semiclassical extended Thomas-Fermi approach under frozen density approximation. Here, within the DCM, the Skyrme forces used are SLy4, SkM*, and, KDE0(v1). The DCM makes use of a single parameter, the neck-length parameter ΔR that takes different values for different processes at a given temperature and provides an excellent fit to the measured data, independently of the choice of Skyrme force used. We make predictions of probable fusion-fission and quasifission mass regions of fragments and then calculate the evaporation residue cross sections σ_{ER} for experimentally unobserved neutron channels. Further, the product $P_{\text{CN}}P_{\text{Surv}}$ of compound nucleus (CN) fusion probability P_{CN} and survival probability P_{Surv} is calculated to determine the reduced evaporation residue cross section $\sigma_{\text{ER}}/\sigma_{\text{fusion}}$, denoted as $\sigma_{\text{ER}}^{\text{reduced}}$, and we have seen that P_{Surv} is the main dominant factor in the product $P_{\text{CN}}P_{\text{Surv}}$. To this end, we have analyzed the effects of mass asymmetry and isospin effect of target nucleus on the σ_{ER} and have found that the σ_{ER} for the production of superheavy element Fl* increases slowly with increasing neutron number of the target nucleus. We have also searched for all possible target-projectile combinations forming the hot compound nucleus Fl* at the excitation energy E^* for compact-hot configurations and have also calculated the fusion evaporation residue cross sections for the proposed new reactions synthesizing Fl.

DOI: [10.1103/PhysRevC.107.014610](https://doi.org/10.1103/PhysRevC.107.014610)

I. INTRODUCTION

At present, in both the nuclear experiment and theory, the production and spectroscopic study of superheavy nuclei (SHN) are one of the most important topics. Owing to the small lifetimes and extremely low probabilities of their production, the final cross sections are extremely small. One can make trustworthy predictions of probabilities for the synthesis of even heavier, still not invented SHN. The complete fusion reactions with ^{48}Ca ions as projectiles have been successfully employed to synthesize SHN having charge numbers $Z = 112 - 118$ in the neutron evaporation channels (xn -evaporation channels) and to proceed to the “island of stability” of SHN estimated at $Z = 114 - 126$ and neutron numbers $N = 172 - 184$ through the extrapolation based on the nuclear shell models [1].

It is highly relevant to analyze the systematics of various target-projectile (t-p) combinations forming the same compound nucleus (CN) system. The reaction dynamics concerning CN formation/decay are significantly affected by the asymmetry of reaction, deformation, orientations, and shape of the colliding nuclei. Consequently, the right knowledge of these parameters is greatly necessary for the successful study of the dynamical description of a nuclear system. Nowadays

various theoretical models such as the two step model [2], the fusion-by-diffusion model [3], nuclear collectivization model [4], the Langevin model [5,6], time-dependent Hartree-Fock [7–9], dinuclear system (DNS) [10,11], and the dynamical cluster-decay model (DCM) [12,13] are available to describe the fusion dynamics of heavy-ion-induced reactions. The DCM can successfully describe the mass and charge asymmetry of the CN system, the dissipation of kinetic energy and angular momentum ℓ , and prediction of the production cross sections of SHN in fusion evaporation reactions.

Recently, we have applied the DCM to study the decay of compound nuclear system $^{286}\text{Cn}^*(Z = 112)$ synthesized via $^{238}\text{U} + ^{48}\text{Ca}$ and have studied the possible fusion-fission (ff) and quasifission (qf) mass regions of fragments and also searched all the possible t-p combinations forming $^{286}\text{Cn}^*$ at various CN excitation energies E^* for hot compact configurations. A nice fitting of the data to evaporation residue cross sections via $3n$ - and $4n$ -decay channels was obtained [14]. The promising results of Ref. [14] prompted us to extend the work to more heavier SHN flerovium Fl*($Z = 114$). It is a transactinide in the p -block and seventh period of the periodic table and it is the heaviest known member of the carbon group, and the last element whose chemistry has been investigated. Initial chemical studies indicated that it was unexpectedly

volatile for a group 14 element [15]; even seemed to exhibit properties similar to noble gases [16,17]. More recent results show that it interacts with gold as with copernicium (Cn), has metallic properties consistent with being the heavier homologue of lead, and is the least reactive metal in group 14 [18]. Fl is predicted to be situated near the center of the theorized island of stability, and it is expected that heavier Fl isotopes, especially the possibly magic $^{298}\text{Fl}^*$, may have even longer half-lives [19].

One of the major motivations behind this work is to study the influence of the entrance channel on the synthesis of various isotopes of CN Fl^* . The entrance channel dependence of the σ_{ER} for SHN has been of great concern for several reasons. First, to search for the optimal condition of synthesis, it is necessary to study the dependence of the σ_{ER} on the isospin composition of colliding nuclei. Consequently, the influence of the neutron number (or the N/Z ratio) of the projectile and target on the calculated σ_{ER} are studied. Second, the role of the nuclear ground state deformation, nuclear structure, and Coulomb barrier can be ascertained by the comparison of the experimental σ_{ER} obtained from the reactions with different projectile and target nucleus leading to the formation of the same CN.

Theoretically, the reaction $^{244}\text{Pu} + ^{48}\text{Ca}$ has been a focus area of comprehensive study by Gupta and collaborators [20] for the decay of CN $^{292}\text{Fl}^*$ using nuclear proximity potential due to Blocki *et al.* [21] in the dynamical cluster-decay model (DCM), including the effects of both deformations and orientations degrees of freedom of the colliding or outgoing nuclei.

In this paper, we present the study of dynamics of various isotopes of the SHN $^{287,288,290,292}\text{Fl}^*$ compound systems formed in $^{239,240,242,244}\text{Pu} + ^{48}\text{Ca}$ reactions, by using three Skyrme forces specifically, newer KDE0(v1), and conventional SLy4 and SkM* in the DCM via the Skyrme nucleus-nucleus interaction potential which is obtained from the semiclassical extended Thomas-Fermi (ETF) approach in the Skyrme energy density formalism (SEDF) under the frozen density approximation. The nucleus-nucleus interaction potential derived from the SEDF is advantageous over the potential which is derived due to Blocki *et al.* The former one allows the use of different Skyrme forces, having different barrier characteristics, to introduce the barrier modification effect for a best fit to data via different Skyrme forces. Whereas, the latter one has fixed barrier height, position, and curvature. In a nutshell, greater flexibility for a better comparison of data is provided by the Skyrme forces as they nicely fit different ground-state properties of nuclei from different mass regions [20,22].

We here made our calculations for both the cold elongated and hot compact configurations, but the hot compact configuration appears to have a preference for $^{292}\text{Fl}^*$, as it supports symmetric fission [20,23,24], in complete agreement with experiments. Contrastingly, cold elongated configuration for $^{292}\text{Fl}^*$ gives rise to asymmetric fission, which is not supported by experiments. Also exactly the same t-p combinations, as are used in the experiments [24–27], plus a few more, are suggested for the synthesis of CN $^{287,288,290,292}\text{Fl}^*$ on the basis of Skyrme force included in the DCM.

Thus, the objective of the paper is at least threefold: First, we search, based on the choice of the orientation degree of freedom (“hot” or “cold” configuration), whether the CN $^{292}\text{Fl}^*$ encounters fission through symmetric or asymmetric mass distribution. Second, we search for the compact “hot” reaction partners for the synthesis of the $^{287,288,290,292}\text{Fl}^*$ compound nuclear systems, which could be employed along with the one already used in the experiments. Third, we explored the reaction dynamics of the decay of $^{287,288,290,292}\text{Fl}^*$ by reproducing the measured excitation functions for $2n-5n$ emission (the ER cross sections $\sigma_{\text{ER}} = \sum_{(X=2-5)} \sigma_{Xn}$, as a function of CN excitation energy E^*) in terms of a single parameter ΔR of the model DCM with all three Skyrme forces in “hot” configurations. The so-obtained results are compared with the available experimental data [24–27] and other theoretical works [28,29]. Further, in order to determine the reduced evaporation residue cross section $\sigma_{\text{ER}}/\sigma_{\text{fusion}}$, denoted by $\sigma_{\text{ER}}^{\text{reduced}}$, we have calculated the product $P_{\text{CN}}P_{\text{surv}}$ of CN-fusion probability P_{CN} and survival probability P_{surv} . Here, (total) fusion cross section σ_{fusion} is given as a sum of CN-formation cross section σ_{CN} and non-CN cross section σ_{nCN} for each reaction. The σ_{CN} is the sum of evaporation residue cross section σ_{ER} and fusion-fission cross section σ_{ff} while σ_{nCN} is the difference between measured and calculated σ_{fusion} [30].

The paper is organized into four sections as follows. Section II gives a brief detail of the model DCM and the very relevant details of the nucleus-nucleus interaction potential in Skyrme energy density formalism (SEDF) based on semiclassical ETF approach under frozen density approximation. Section III presents the study of the role of “hot-compact” configurations, the formation of $^{287,288,290,292}\text{Fl}^*$, and their decay via $2n-5n$ channels by using the DCM with Skyrme force-based nuclear interaction. In Sec. IV conclusions of the present study are briefly summarized.

II. THEORETICAL FORMALISM

In this section, we first introduce the well-known quantum mechanical fragmentation theory (QMFT) [31–36] and then describe the very essential details of the DCM based on QMFT and SEDF in the semiclassical ETF approach.

A. Dynamical cluster-decay model (DCM)

When a projectile having energy larger than the barrier energy is projected onto some target, the CN formation takes place. If the so-formed nuclear system is heavy enough, i.e., CN mass number $A_{\text{CN}} \geq 200$ then the most probable decay mode is fragment emission. The process of decay through fragments can be described very well within the framework of the DCM based on QMFT.

The DCM [12,13,22,37–53] is worked out in terms of collective coordinates of mass (and charge) asymmetry $\eta = (A_1 - A_2)/(A_1 + A_2)$ [and $\eta_Z = (Z_1 - Z_2)/(Z_1 + Z_2)$], and relative separation R , the multipole deformations $\beta_{\lambda i}$, and orientations θ_i ($i = 1, 2$) of two nuclei in the same plane. Here, A_1 and A_2 (Z_1 and Z_1) are the mass (charge) numbers of fragments and $A_1 + A_2 (= A_{\text{CN}})$ is the mass number of the CN. In the DCM, using decoupled approximation to R and η motion,

we define the compound nucleus decay cross section in terms of partial wave analysis, the compound nucleus decay or the fragments production cross section is

$$\sigma = \sum_{\ell=0}^{\ell_{\max}} \sigma_{\ell} = \frac{\pi}{k^2} \sum_{\ell=0}^{\ell_{\max}} (2\ell + 1) P_0^{\ell} P_{\ell}; \quad k = \sqrt{\frac{2\mu E_{\text{c.m.}}}{\hbar^2}}, \quad (1)$$

where the preformation probability P_0^{ℓ} refers to η motion and the penetrability P_{ℓ} to R motion. ℓ_{\max} is the maximum angular momentum, fixed here for the light particle cross section approaching zero, i.e., $\sigma_{\text{ER}}(\ell) \rightarrow 0$ at $\ell = \ell_{\max}$ and $\mu = [A_1 A_2 / (A_1 + A_2)] m = \frac{1}{4} A m (1 - \eta^2)$ is the reduced mass with m the nucleon mass, $E_{\text{c.m.}}$, the entrance channel center of mass (c.m.) energy.

P_0 for each ℓ is the solution of the stationary Schrödinger equation in η , at the fixed $R = R_a$, the first turning point(s) of the penetration path(s) (illustrated, e.g., in Fig. 2 for different ℓ values),

$$\left[-\frac{\hbar^2}{2\sqrt{B_{\eta\eta}}} \frac{\partial}{\partial \eta} \frac{1}{\sqrt{B_{\eta\eta}}} \frac{\partial}{\partial \eta} + V(\eta) \right] \psi^{\nu}(\eta) = E_{\eta}^{\nu} \psi^{\nu}(\eta) \quad (2)$$

with $\nu = 0, 1, 2, 3, \dots$ referring to ground-state ($\nu = 0$) and excited-states solutions. Above V is the potential which in general depends on various quantities like η , R , ℓ , T , β , θ , etc., however, only η dependence is explicitly shown here for brevity. The mass parameters $B_{\eta\eta}$ in Eq. (2) are the smooth classical hydrodynamical masses [54], used for simplicity. In principle, the shell corrected masses, like the cranking masses, should be used. The probability

$$P_0(A_i) = |\psi(\eta(A_i))|^2 \sqrt{B_{\eta\eta}} \frac{2}{A}, \quad (3)$$

where, for a Boltzmann-like function,

$$|\psi|^2 = \sum_{\nu=0}^{\infty} |\psi^{\nu}|^2 \exp(-E^{\nu}/T). \quad (4)$$

P_0 contains the structure information of compound nucleus, which enter via the fragmentation potential.

The penetrability P_{ℓ} is the Wentzel-Kramers-Brillouin (WKB) integral between R_a and R_b ,

$$P_{\ell} = \exp \left[-\frac{2}{\hbar} \int_{R_a}^{R_b} \{2\mu[V(R, \ell) - Q_{\text{eff}}]\}^{1/2} dR \right] \quad (5)$$

with R_b as the second turning point, satisfying

$$V(R_a, \ell) = V(R_b, \ell) = Q_{\text{eff}}(T, \ell) = \text{TKE}(T). \quad (6)$$

Here, $\text{TKE}(T)$ is the temperature dependent total kinetic energy. The ℓ dependence of R_a is defined by

$$V(R_a, \ell) = Q_{\text{eff}}(T, \ell = \ell_{\min}), \quad (7)$$

which means that R_a , given by Eq. (7), is the same for all ℓ values, and that $V(R_a, \ell)$ acts like an effective Q value, $Q_{\text{eff}}(T, \ell)$, given by the total kinetic energy $\text{TKE}(T)$. ℓ_{\min} refers to the minimum value that starts to contribute to the WKB integral. Apparently, as the ℓ value increases, the $Q_{\text{eff}}(T)$ value [=TKE(T)] increases and hence $V(R_a, \ell)$ increases (see Fig. 2).

For the decay of a hot compound nucleus, we use the following postulate for the first turning point:

$$\begin{aligned} R_a(T) &= R_1(\alpha_1, T) + R_2(\alpha_2, T) + \Delta R(T) \\ &= R_f(\alpha_1, \alpha_2, T) + \Delta R(T) \end{aligned} \quad (8)$$

with $\Delta R(T)$ as the neck-length parameter, assimilating the neck formation effects [55,56]. This method of introducing a neck-length parameter is similar to that used in both the scission-point [57] and saddle-point [58,59] statistical fission models. Note that $R_a(T)$ in Eq. (8) are α dependent since $R_f(T)$ are different for different α values.

Then, the deformation and orientation dependent fragmentation potential $V(\eta)$ in Eq. (2), at any temperature T , is given as

$$\begin{aligned} V(\eta, T) &= \sum_{i=1}^2 V_{\text{LDM}}(A_i, Z_i, T) + \sum_{i=1}^2 \delta U \exp\left(-\frac{T^2}{T_0^2}\right) \\ &\quad + V_C(R, Z_i, \beta_{\lambda_i}, \theta_i, T) + V_{\ell}(R, A_i, \beta_{\lambda_i}, \theta_i, T) \\ &\quad + V_N(R, A_i, \beta_{\lambda_i}, \theta_i, T). \end{aligned} \quad (9)$$

Here, V_{LDM} is the T -dependent liquid drop energy of Davidson *et al.* [60] with its constants at $T = 0$ refitted in Refs. [40,41,45,61]. The shell corrections δU calculations are done with the help of the ‘‘empirical’’ estimates of Myers and Swiatecki [62]. The Coulomb potential for a multipole-multipole interaction between two separated, deformed and oriented, nuclei is

$$\begin{aligned} V_C &= \frac{Z_1 Z_2 e^2}{R} + 3Z_1 Z_2 e^2 \sum_{\lambda, i=1,2} \frac{R_i^{\lambda}(\alpha_i, T)}{(2\lambda + 1)R^{\lambda+1}} \\ &\quad \times Y_{\lambda}^{(0)}(\theta_i) \left[\beta_{\lambda_i} + \frac{4}{7} \beta_{\lambda_i}^2 Y_{\lambda}^{(0)}(\theta_i) \right] \end{aligned} \quad (10)$$

with θ_i and α_i are the angles as shown in Fig. 1 and the angular momentum dependent potential

$$V_{\ell} = \frac{\hbar^2 \ell(\ell + 1)}{2I} \quad (11)$$

with $I = I_S = \mu R^2 + \frac{2}{5} A_1 m R_1^2(\alpha_1, T) + \frac{2}{5} A_2 m R_2^2(\alpha_2, T)$, the moment of inertia in sticking limit. V_N is the nuclear interaction potential discussed in next subsection.

The temperature T is related to the incoming center-of-mass energy $E_{\text{c.m.}}$ or the compound nucleus excitation energy E^* via the entrance channel Q_{in} value as

$$E^* = E_{\text{c.m.}} + Q_{\text{in}} = \frac{1}{a_c} A T^2 - T \quad (T \text{ in MeV}) \quad (12)$$

with a_c (a constant)=9 or 10, respectively, for intermediate mass or superheavy systems. $Q_{\text{in}} = B_1 + B_2 - B_{\text{CN}}$ with binding energies B 's taken from [63].

Apparently, in the DCM, both the light particles ($A_2 \leq 4$ or 5), referring to ER, and the complex, heavy mass fragments, referring to fusion-fission (ff) processes, are treated as the dynamical collective mass motion of preformed clusters or fragments through the barrier. The same formula [Eq. (1)] is also applicable to the noncompound, competing qf decay

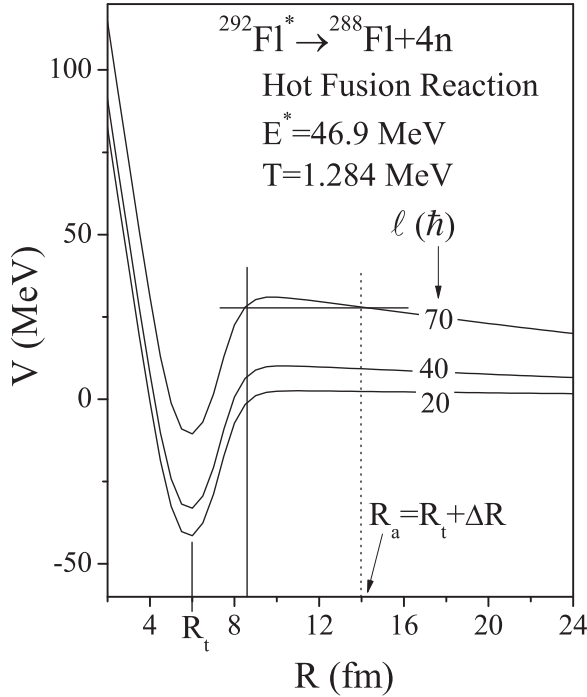


FIG. 1. Scattering potentials $V(R, \ell)$ for $^{292}\text{Fl}^* \rightarrow ^{288}\text{Fl}^* + 4n$ at excitation energy $E^* = 46.9$ MeV and at fixed temperature $T = 1.284$ MeV at different angular momentum ℓ values varying from $\ell_{\min} = 20\hbar$ to $\ell_{\max} = 70\hbar$ for the Skyrme force SLy4 ($\ell < \ell_{\min}$ do not contribute).

channel σ_{qf} , where $P_0 = 1$ for the incoming channel, since both the target and projectile nuclei can be considered to have not yet lost their identity.

$$\begin{aligned}
 H(\rho, \tau, \vec{J}) = & \frac{\hbar^2}{2m} \tau + \frac{1}{2} t_0 \left[\left(1 + \frac{1}{2} x_0 \right) \rho^2 - \left(x_0 + \frac{1}{2} \right) (\rho_n^2 + \rho_p^2) \right] + \frac{1}{2} \sum_{i=1}^3 t_{3i} \rho^{\alpha_i} \left[\left(1 + \frac{1}{2} x_{3i} \right) \rho^2 - \left(x_{3i} + \frac{1}{2} \right) (\rho_n^2 + \rho_p^2) \right] \\
 & + \frac{1}{4} \left[t_1 \left(1 + \frac{1}{2} x_1 \right) + t_2 \left(1 + \frac{1}{2} x_2 \right) \right] \rho \tau - \frac{1}{4} \left[t_1 \left(x_1 + \frac{1}{2} \right) - t_2 \left(x_2 + \frac{1}{2} \right) \right] (\rho_n \tau_n + \rho_p \tau_p) \\
 & + \frac{1}{16} \left[3t_1 \left(1 + \frac{1}{2} x_1 \right) - t_2 \left(1 + \frac{1}{2} x_2 \right) \right] (\vec{\nabla} \rho)^2 - \frac{1}{16} \left[3t_1 \left(x_1 + \frac{1}{2} \right) + t_2 \left(x_2 + \frac{1}{2} \right) \right] [(\vec{\nabla} \rho_n)^2 + (\vec{\nabla} \rho_p)^2] \\
 & - \frac{1}{2} W_0 [\rho \vec{\nabla} \vec{J} + \rho_n \vec{\nabla} \vec{J}_n + \rho_p \vec{\nabla} \vec{J}_p] - C \left[\frac{1}{16} (t_1 x_1 + t_2 x_2) \vec{J}^2 - \frac{1}{16} (t_1 - t_2) (\vec{J}_p^2 + \vec{J}_n^2) \right]. \quad (15)
 \end{aligned}$$

Here, $\rho = \rho_n + \rho_p$, $\tau = \tau_n + \tau_p$, and $\vec{J} = \vec{J}_n + \vec{J}_p$ are the nuclear, kinetic energy, and spin-orbit densities for the composite system, respectively. m is the nucleon mass, and x_j , t_j ($j = 0, 1, 2$), x_{3i} , t_{3i} , α_i , ($i = 1, 2, 3$), W_0 and C are the Skyrme force parameters, fitted by different authors to reproduce ground state properties of various nuclei. For the forces [68] like SLy4 and SkM*, some constants [C , x_{3i} , t_{3i} , and α_i ($i = 2, 3$)] are zero, and $t_{31} = \frac{1}{6} t_3$, $x_{31} = x_3$, and $\alpha_1 = \alpha$. For the force KDE0(v1), we have $C = 1$ and six additional constants (two each of x_{3i} , t_{3i} , and α_i), determined by a fit to several properties of the normal and isospin-rich nuclei [66,69].

The kinetic energy density in the ETF method, considered here up to second order terms for reasons of being enough for numerical convergence [70], is ($q = n$ or p)

$$\tau_q(\vec{r}) = \frac{3}{5} (3\pi^2)^{2/3} \rho_q^{5/3} + \frac{1}{36} \frac{(\vec{\nabla} \rho_q)^2}{\rho_q} + \frac{1}{3} \Delta \rho_q + \frac{1}{6} \frac{\vec{\nabla} \rho_q \vec{\nabla} f_q + \rho_q \Delta f_q}{f_q} - \frac{1}{12} \rho_q \left(\frac{\vec{\nabla} f_q}{f_q} \right)^2 + \frac{1}{2} \rho_q \left(\frac{2m}{\hbar^2} \right)^2 \left(\frac{W_0 \vec{\nabla}(\rho + \rho_q)}{2 f_q} \right)^2 \quad (16)$$

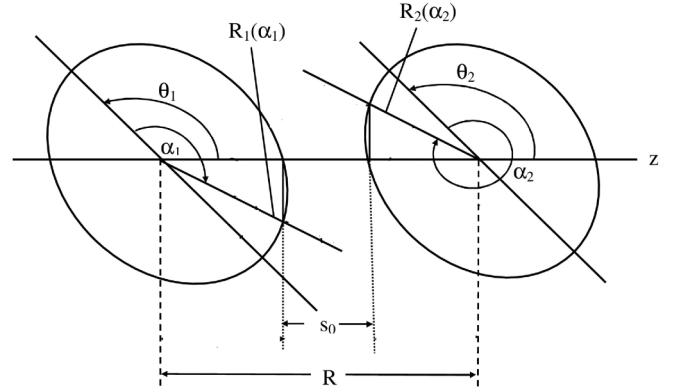


FIG. 2. Schematic diagram showing the angles (θ_1 , θ_2 , α_1 , and α_2).

B. Nuclear interaction potential based on SEDF in the semiclassical ETF approach

Nuclear interaction potential within the energy density formalism is defined as (see, e.g., [64,65])

$$V_N(R) = E(R) - E(\infty), \quad (13)$$

i.e., the nucleus-nucleus interaction potential as a function of separation distance, $V_N(R)$, is the difference of the energy expectation value E of the colliding nuclei when these are overlapping (at a finite separation distance R) and are completely separated (at $R = \infty$), where

$$E = \int H(\vec{r}) d\vec{r}. \quad (14)$$

For the Skyrme interaction the energy density $H(\vec{r})$ is an algebraic function of the nucleon densities $\rho_n(\rho_p)$, the kinetic energy density $\tau_n(\tau_p)$, and spin-orbit density $\vec{J}_n(\vec{J}_p)$. The Skyrme Hamiltonian density is defined as [66,67]

with f_q as the effective mass form factor

$$f_q(\vec{r}) = 1 + \frac{2m}{\hbar^2} \frac{1}{4} \left\{ t_1 \left(1 + \frac{x_1}{2} \right) + t_2 \left(1 + \frac{x_2}{2} \right) \right\} \rho(\vec{r}) - \frac{2m}{\hbar^2} \frac{1}{4} \left\{ t_1 \left(x_1 + \frac{1}{2} \right) - t_2 \left(x_2 + \frac{1}{2} \right) \right\} \rho_q(\vec{r}). \quad (17)$$

Note that both τ_q and f_q are each functions of ρ_q and/or ρ only.

The spin-orbit density \vec{J} is a purely quantal property, and hence has no contribution in the lowest Thomas-Fermi (TF) order. However, at the ETF level, the second order contribution gives

$$\vec{J}_q(\vec{r}) = -\frac{2m}{\hbar^2} \frac{1}{2} W_0 \frac{1}{f_q} \rho_q \vec{\nabla}(\rho + \rho_q), \quad (18)$$

which is also a function of ρ_q and/or ρ alone.

The densities for the composite system under the frozen density approximation used here are [71]

$$\begin{aligned} \rho &= \rho_1 + \rho_2, \\ \tau(\rho) &= \tau_1(\rho_1) + \tau_2(\rho_2), \\ \vec{J}(\rho) &= \vec{J}_1(\rho_1) + \vec{J}_2(\rho_2) \end{aligned} \quad (19)$$

with $\rho_i = \rho_{in} + \rho_{ip}$, $\tau_i(\rho_i) = \tau_{in}(\rho_{in}) + \tau_{ip}(\rho_{ip})$, and $\vec{J}_i(\rho_i) = \vec{J}_{in}(\rho_{in}) + \vec{J}_{ip}(\rho_{ip})$.

Further, we have calculated the CN-fusion probability P_{CN} and the CN survival probability P_{surv} against fission, i.e., the probability of a fused system to de-excite by the emission of neutrons or light particles (LPs), equivalently, the evaporation residue ER, rather than fission, each given by

$$P_{\text{CN}} = \frac{\sigma_{\text{CN}}}{\sigma_{\text{fusion}}} = 1 - \frac{\sigma_{\text{nCN}}}{\sigma_{\text{fusion}}} \quad (20)$$

and

$$P_{\text{surv}} = \frac{\sigma_{\text{ER}}}{\sigma_{\text{CN}}} = 1 - \frac{\sigma_{\text{ff}}}{\sigma_{\text{CN}}}, \quad (21)$$

where the (total) fusion cross section $\sigma_{\text{fusion}} = \sigma_{\text{CN}} + \sigma_{\text{nCN}}$, with σ_{CN} as the CN formation cross section, given as the sum of evaporation residue and fusion-fission (ff) cross sections ($\sigma_{\text{CN}} = \sigma_{\text{ER}} + \sigma_{\text{ff}}$) and σ_{nCN} as the noncompound nucleus (nCN) cross section, such as the qf, deep-inelastic collisions/orbiting (DIC), incomplete fusion (ICF), or pre-equilibrium decay [30]. Evidently, P_{CN} takes care of the nCN effects, and P_{surv} takes care of the ff process. Therefore,

$$\sigma_{\text{ER}} = \sigma_{\text{CN}} P_{\text{surv}} = \sigma_{\text{fusion}} P_{\text{CN}} P_{\text{surv}}. \quad (22)$$

Apparently, the product $P_{\text{CN}} P_{\text{surv}}$ gives σ_{ER} , relative to σ_{fusion} , referred here as ‘‘reduced’’ evaporation residue cross section $\sigma_{\text{ER}}/\sigma_{\text{fusion}}$, denoted by $\sigma_{\text{ER}}^{\text{reduced}}$. Noting that for the limiting case of $P_{\text{CN}} = 1$ ($\sigma_{\text{nCN}} = 0$) the reduced-ER cross section depends on the variation of P_{surv} and for $P_{\text{surv}} = 1$ ($\sigma_{\text{ff}} = 0$) it depends on the variation of P_{CN} , it will be interesting to study the dependence of product $P_{\text{CN}} P_{\text{surv}}$ or the reduced-ER cross section $\sigma_{\text{ER}}/\sigma_{\text{fusion}}$ on CN excitation energy E^* [30].

III. CALCULATIONS AND DISCUSSION

In this section, we present the results of our calculation for σ_{ER} for synthesis and decay of various isotopes of CN FI* and also the results of CN formation probability P_{CN} and survival probability P_{surv} . The comparison of the σ_{ER} measured for different mass asymmetry reactions but leading to the same compound nucleus allows us to analyze the importance of the entrance channel effects on the fusion mechanism. The σ_{ER} is mainly dependent on the fusion and survival probabilities of the compound nucleus. The survival probability increases with increasing neutron number of the target in addition to the even odd effect. However, the fusion probability changes with neutron number of the target irregularly, which depends on the details of the driving potential [28]. For this, first we identify all the possible t-p combinations [minima in potential energy surface (PES)] at hot or cold orientations, i.e., hot-compact or cold-elongated configurations leading to the formation of CN FI* at a fixed temperature T and among these, the most optimum reaction giving largest fusion cross section. The best choice of either hot or cold configuration depends on the calculated yields compared with measured fission mass distribution. Then in the next subsection, the decay of FI* via $2n, 3n, 4n$, and $5n$ emissions is discussed. We have performed calculations using the DCM with nuclear interaction potential obtained from the SEDF-based ETF method for three illustrative Skyrme forces SLy4, SkM*, and KDE0(v1).

A. Synthesis of compound nuclei $^{287,288,290,292}\text{Fl}^*$

In order to investigate the synthesis of various FI isotopes, we calculate the fragmentation potential $V(\eta)$ for all possible t-p combinations (η values) forming optimum hot fusion configurations (or cold fusion configurations) at a fixed $\Delta R = 0.1$ fm for each Skyrme force. This is shown in Fig. 3 for hot and in Fig. 4 for cold configurations of the compound nucleus $^{292}\text{Fl}^*$, using (a) SLy4, (b) SkM*, and (c) KDE0(v1) Skyrme forces. We notice from each of these two figures that all minima are nearly common for all three forces, i.e., all three forces behave nearly alike since almost the same t-p combinations refer to the minimum. Interestingly, in Fig. 3 for hot-fusion configurations, for all three cases, the potential energy minima occur at the symmetric fragmentation [for instance, there are minima which correspond to ^{85}Se , ^{87}Br and ^{205}Au , ^{207}Tl in Fig. 3(a)], whereas no such minima occur in Fig. 4 for cold-fusion configurations. The above results from fragmentation potentials can be better understood in terms of the corresponding production yields for the two cases (hot and cold fusion processes), shown in Figs. 5 and 6, respectively, for the fragmentation potentials in Figs. 3 and 4. We notice that, independent of the Skyrme force used, there is a strong dissimilarity in the hot and cold paths of fragmentation, and the symmetric fission mass distribution is obtained only for the hot fusion case, in complete accordance with experiments [24,25,72]. Hence, in the following, we focus only on hot fusion configurations, i.e., Figs. 3 and 5. The resulting t-p combinations, referring to minima in PES for hot-fusion configuration, marked in Fig. 3, are listed in Table I for Skyrme force KDE0(v1), together with

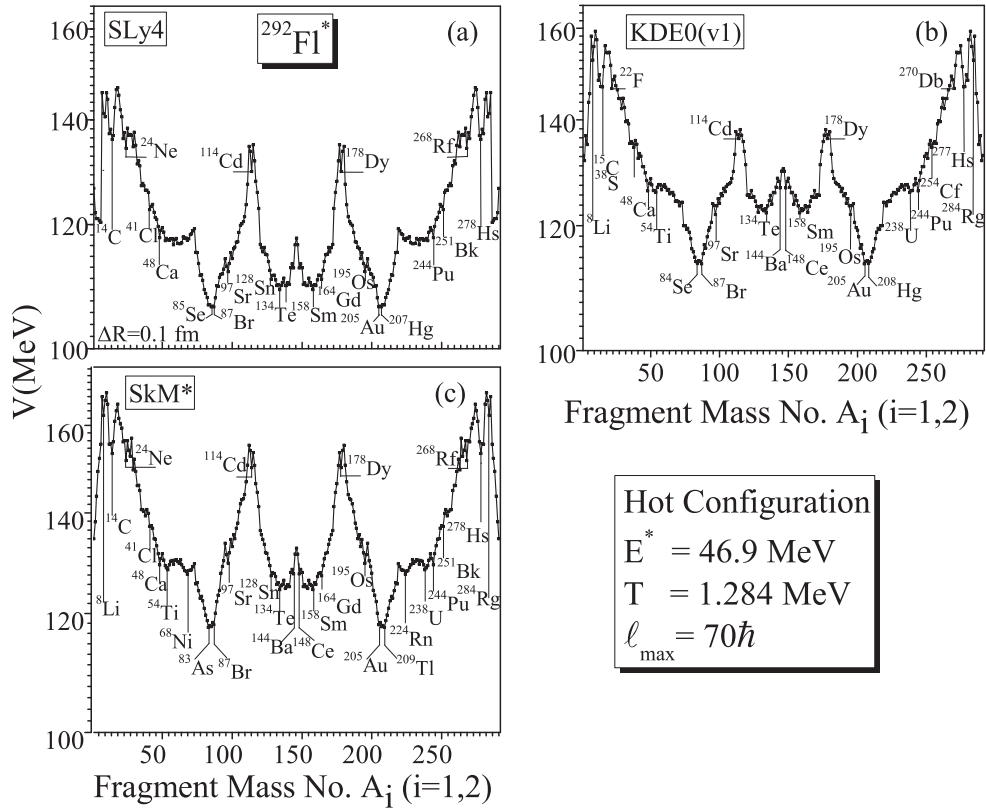


FIG. 3. Mass fragmentation potential $V(A_i)$, $i = 1, 2$ at $\ell = \ell_{\max}$ for the formation of CN $^{292}\text{Fl}^*$ at $T = 1.284$ MeV corresponding to $E^* = 46.9$ MeV, calculated at fixed $R = R_t + \Delta R$ with $\Delta R = 0.1$ fm, and with β_2 deformations and “optimum hot” orientations included for all possible t-p combinations, using Skyrme forces (a) SLy4, (b) SkM*, and (c) KDE0(v1).

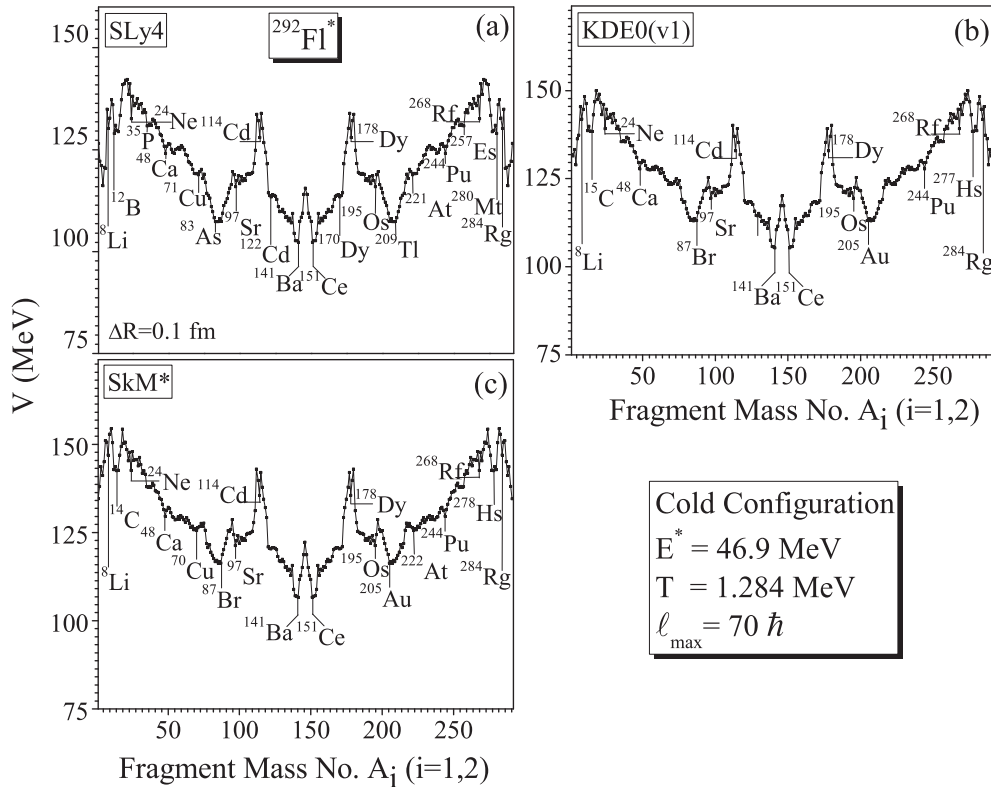


FIG. 4. Same as Fig. 3, but for “optimum cold” orientations.

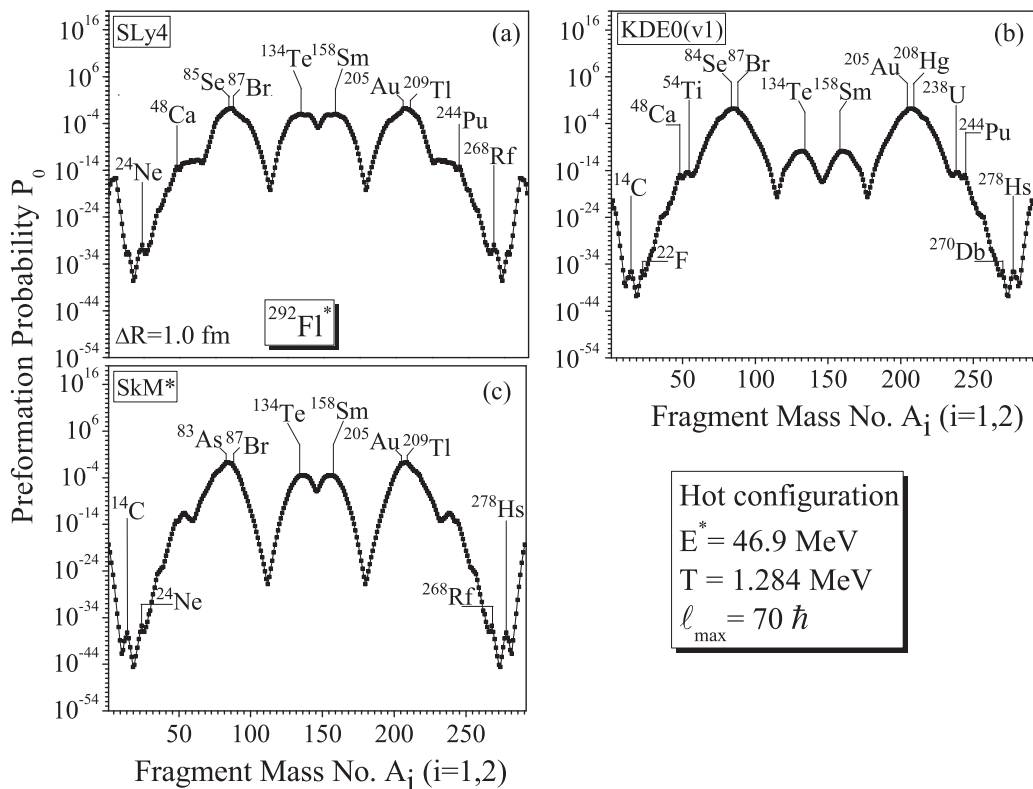


FIG. 5. Preformation yields for “hot configurations” referring to the fragmentation potentials in Fig. 3.

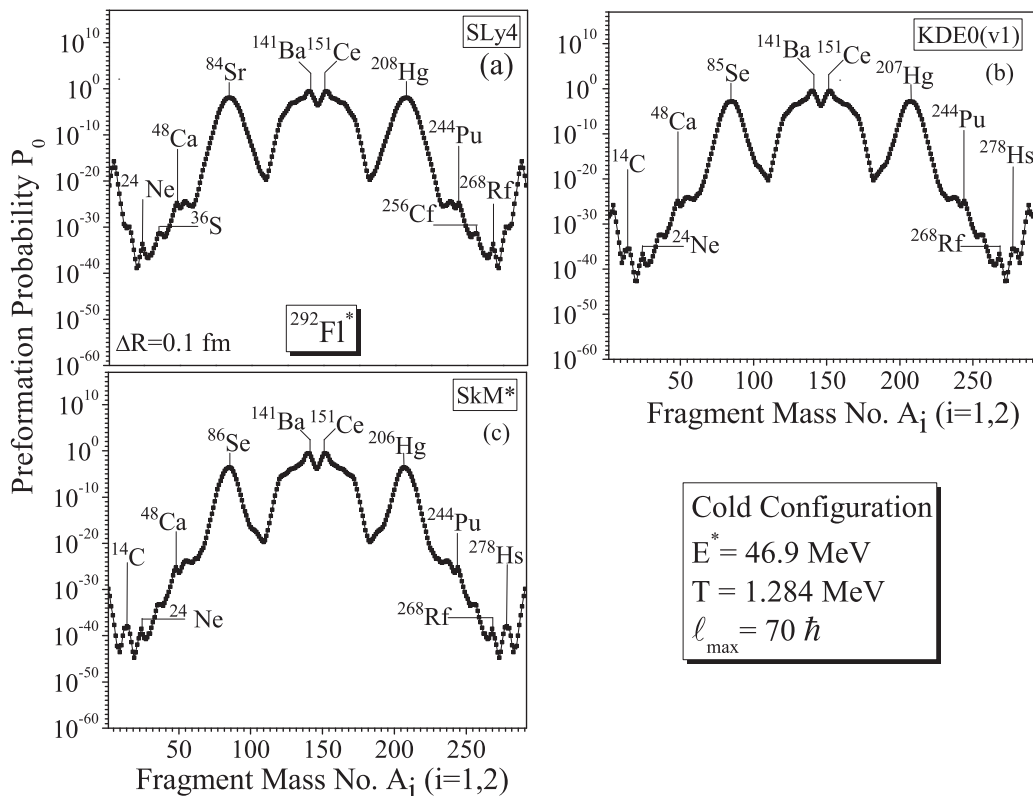


FIG. 6. Preformation yields for “cold configurations” referring to the fragmentation potentials in Fig. 4.

TABLE I. The t-p combinations (A_1, A_2) referring to minima in potential energy surface (PES) at $\ell_{\max} = 70\hbar$ and for quadrupole deformed and oriented nuclei forming the CN $^{292}\text{Fl}^*$ at $T = 1.284$ MeV ($E^* = 46.9$ MeV) for the illustrative SkM* Skyrme force, and their other characteristic properties.

Reactions $A_1 + A_2$	β_{21}	β_{22}	V_B (MeV)	R_B (fm)
$^{284}\text{Rg} + ^8\text{Li}$	0.099	-0.09	28.13	10.13
$^{278}\text{Hs} + ^{14}\text{C}$	0.108	-0.016	74.761	9.39
$^{268}\text{Rf} + ^{24}\text{Ne}$	0.221	-0.215	106.083	10.16
$^{263}\text{Md} + ^{29}\text{Al}$	0.22	0.0	141.62	10.94
$^{254}\text{Cf} + ^{38}\text{S}$	0.226	0.0	183.922	12.0
$^{244}\text{Pu} + ^{48}\text{Ca}$	0.224	0.0	207.526	12.54
$^{238}\text{U} + ^{54}\text{Ti}$	0.215	0.0	217.692	12.81
$^{224}\text{Rn} + ^{68}\text{Ni}$	0.163	0.018	251.278	13.09
$^{195}\text{Os} + ^{97}\text{Sr}$	0.127	0.349	275.874	13.23
$^{164}\text{Gd} + ^{128}\text{Sn}$	0.301	0.0	341.946	12.6
$^{158}\text{Sm} + ^{134}\text{Te}$	0.279	0.0	342.39	12.7

their other characteristics such as quadrupole deformations β_{2i} [63], and calculated barrier heights V_B and positions R_B for optimum hot-compact orientations. We notice that, in addition to the ^{48}Ca -induced reaction, there are a few other possibilities, specifically, $^{284}\text{Rg} + ^8\text{Li}$, $^{278}\text{Hs} + ^{14}\text{C}$, $^{268}\text{Rf} + ^{24}\text{Ne}$, $^{263}\text{Md} + ^{29}\text{Al}$, $^{254}\text{Cf} + ^{38}\text{S}$, $^{238}\text{U} + ^{54}\text{Ti}$, $^{224}\text{Rn} + ^{68}\text{Ni}$, $^{195}\text{Os} + ^{97}\text{Sr}$, $^{164}\text{Gd} + ^{128}\text{Sn}$, $^{158}\text{Sm} + ^{134}\text{Te}$, and $^{154}\text{Nd} + ^{138}\text{Xe}$ which may be suggested, in principle, for future experiments. However because of the technical constraints on the preparation of targets, the best suited t-p combinations suggested here are $^{254}\text{Cf} + ^{38}\text{S}$ and $^{238}\text{U} + ^{54}\text{Ti}$. The previous literary works done by Gupta *et al.* [20] and Li *et al.* [29] also confirm our predictions regarding possible t-p combinations. Additionally, we also predicted t-p combinations for the synthesis of $^{287,288,290,292}\text{Fl}^*$ which are $^{245,246,248}\text{Cm} + ^{42}\text{Ar}$ and $^{230,231,232}\text{Th} + ^{58}\text{Cr}$. Except for these reactions, many other reactions do not survive in the calculated yields due to the reduced shell effect at the considered temperature and low binding energies of incoming reaction partners, so other t-p combinations are not predictable. Hence, a theoretical basis for the choice of t-p combinations for the synthesis of $^{287,288,290,292}\text{Fl}^*$ is provided by QMFT, which have so far been chosen by the experimentalists simply on the basis of availability. The next important question is to make an optimum choice of t-p combination for the production of various isotopes of CN Fl^* with the largest cross section. Note that all t-p combinations considered above referring to minima in PES with hot-compact configurations, which when put together means to say that the interaction radius is smallest and the interaction barrier is lowest [42,43]. Thus, of all the t-p combinations forming the same hot CN system, the optimum t-p refers to the one with lowest interaction barrier and smallest (most compact) interaction radius. Figure 7 shows the interaction (scattering) potentials for all the t-p combinations given in Table I, which appear as minima in Fig. 3(b), together with the one $^{244}\text{Pu} + ^{48}\text{Ca}$, which is used in the experiment.

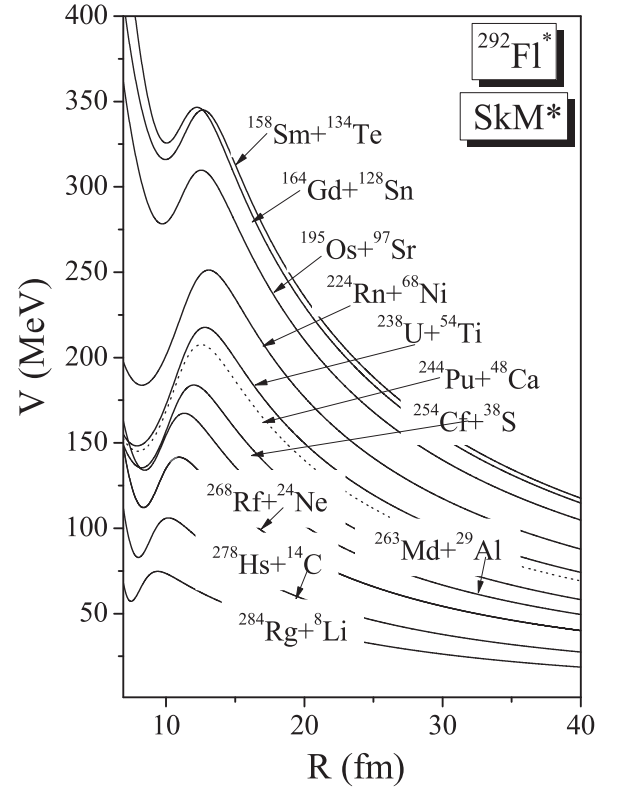


FIG. 7. Scattering potentials $V(R)$ for “hot fusion” reaction valleys with “hot-compact” configurations of Fig. 3(b) at a fixed temperature $T = 1.284$ MeV ($E^* = 46.9$ MeV) and $\ell_{\max} = 70\hbar$, illustrated for SkM* Skyrme force. The potentials for the t-p combinations predicted for future experiments are shown by a solid line while for those used in experiments [24–27] are shown by dotted line.

B. Decay of compound nuclei $^{287,288,290,292}\text{Fl}^*$

In order to study the decay of various Fl isotopes, we estimate the light-particle decay channel cross sections $\sigma_{\sigma_{xn}}$, the fusion-fission cross sections $\sigma_{ff}^{\text{predicted}}$, nCN cross section σ_{nCN} , qf cross sections σ_{qf} using the DCM, for a best fit of ΔR to the measured data on decay of $^{287,288,290,292}\text{Fl}^*$, which is available only for $\sigma_{\sigma_{xn}}$, $x = 2, 3, 4$, and 5. The fitting is done here for the reactions $^{239,240,242,244}\text{Pu} + ^{48}\text{Ca}$ for $E_{\text{lab}} = 235\text{--}250$ MeV using all three chosen Skyrme forces. We have presented our calculated results in Table II and these so-obtained results are compared with experimental data [24–27], and also with results from Bao *et al.* [28] and Li *et al.*'s [29] calculations done by the DNS model. The unobserved (experimentally) $1n$, $2n$, and $4n$ evaporation residue cross sections at different $E^* = 32.5$ MeV to 52.6 MeV are calculated by using the SkM* Skyrme force and the corresponding results are shown in Table IV. Here, it is found that the maximum σ_{ER} is in the $3n$ or $4n$ evaporation channels. This is because the transmission and fusion probability is pretty low due to the low incident energy in $1n$ and $2n$ evaporation channels, and in the $5n$ evaporation channel, fission becomes the main de-excitation mode because of the high excitation energy, in agreement with other work [10]. In addition, we have also calculated P_{CN} and P_{surv} for the $5n$ evaporation channel in the

TABLE II. The excitation functions of $3n$, $4n$, and $5n$ evaporation channels from $^{287,288,290,292}\text{Fl}^*$ due to entrance channels $^{239,240,242,244}\text{Pu} + ^{48}\text{Ca}$ calculated by using the DCM for a best fit of ΔR , at different $E^* = 32.5$ MeV to 52.6 MeV energies for all three chosen Skyrme forces, compared with experimental data [24–27], and also with results from Bao *et al.* [28] and Li *et al.*'s [29] calculations by using the DNS model are shown in this table. The predicted fission cross section ($\sigma_{ff}^{\text{predicted}}$) for CN ^{292}Fl at $E^* = 46.9$ MeV is 4.99×10^{-21} mb for SLy4, 2.49×10^{-13} mb for SkM*, and 3.38×10^{-17} mb for KDE0(v1) Skyrme forces.

E^* (MeV)	xn	T (MeV)	ΔR (fm)			$\sigma_{\text{Calc}}^{\text{DCM}}$ (pb)			$\sigma_{\text{Calc}}^{\text{DNS}}$ (pb)	σ_{exp} (pb)
			SLy4	SkM*	KDE0(v1)	SLy4	SkM*	KDE0(v1)		
$^{244}\text{Pu} + ^{48}\text{Ca}$										
35	$3n$	1.112	1.9041	1.8964	1.8006	0.468	0.47	0.469	1.988	$0.47^{+0.58}_{-0.31}$
35	$4n$	1.112	2.0726	2.2438	2.0272	0.72	0.72	0.369	1.04	$0.37^{+0.05}_{-0.21}$
41	$3n$	1.202	1.9347	1.8654	1.7550	1.7	1.7	1.7	0.214	$1.7^{+2.3}_{-1.1}$
41	$4n$	1.202	2.1323	2.2730	2.0192	5.19	5.16	5.19	1.833	$5.19^{+2.94}_{-1.87}$
46.9	$3n$	1.284	1.8159	1.8262	1.7026	1.12	1.12	1.12	0.01	$1.12^{+2.57}_{-0.93}$
46.9	$4n$	1.284	2.2128	2.2056	1.9660	4.05	4.05	4.05	0.313	$4.05^{+3.15}_{-1.85}$
46.9	$5n$	1.284	2.4696	2.1381	2.1786	0.091	2.11	2.1	0.0598	$2.1^{+0.09}_{-1.54}$
52.6	$3n$	1.359	1.8261	1.8106	1.6950	1.94	1.95	1.95		$1.95^{+0.22}_{-1.6}$
52.6	$4n$	1.359	2.1433	2.1351	1.9105	1.02	1.06	1.06	0.0311	$1.06^{+2.26}_{-0.88}$
52.6	$5n$	1.359	2.1078	2.2419	2.1387	1.13	0.0011	1.13	0.121	$1.13^{+0.06}_{-0.28}$
$^{242}\text{Pu} + ^{48}\text{Ca}$										
32.5	$2n$	1.076	1.8657	1.6509	1.5144	0.5	0.5	0.499		≈ 0.5
32.5	$3n$	1.076	1.8982	2.1182	1.8388	3.2	3.21	3.2	0.42	$3.2^{+1.95}_{-2.2}$
35.3	$3n$	1.116	1.9614	1.9735	1.8209	3.58	3.6	3.6	0.603	$3.6^{+1.99}_{-1.73}$
35.3	$4n$	1.116	2.0409	2.3119	2.0419	1.09	1.09	1.1	0.021	$1.1^{+0.1}_{-0.7}$
40.2	$3n$	1.195	1.9271	1.9248	1.7795	3.59	3.58	3.6	0.278	$3.6^{+2.71}_{-1.51}$
40.2	$4n$	1.195	2.0549	2.3212	2.0435	4.5	4.53	4.5	0.181	$4.5^{+3.6}_{-1.9}$
$^{240}\text{Pu} + ^{48}\text{Ca}$										
38.6	$3n$	1.175	1.8295	1.7262	1.7056	2.5	2.5	2.5	0.23	$2.5^{+2.9}_{-1.4}$
38.6	$4n$	1.175	1.9244	2.0721	1.8232	2.6	2.6	2.6	0.043	$2.6^{+3.3}_{-1.7}$
$^{239}\text{Pu} + ^{48}\text{Ca}$										
37.6	$3n$	1.162	1.7609	1.9768	1.7379	0.229	0.23	0.23	1.689	$0.23^{+0.59}_{-0.20}$

reaction $^{244}\text{Pu} + ^{48}\text{Ca}$ at $E^* = 46.9$ and 52.6 MeV using the SkM* Skyrme force.

Further, for all three Skyrme forces used, Fig. 8 presents the calculated mass fragmentation potential $V(A_i)$, $i = 1, 2$ for the decay of CN $^{292}\text{Fl}^*$ at maximum angular momentum ($\ell_{\text{max}} = 70\hbar$, which is fixed later in Fig. 9), using the best fitted ΔR values (given in the figure caption) at $T = 1.284$ MeV corresponding to the incident energy $E_{\text{lab}} = 250$ MeV of the reaction $^{244}\text{Pu} + ^{48}\text{Ca}$. We note here that this fragmentation potential differs from the one in Fig. 3 since different decay products (here xn) occur in different time scales (different ΔR 's) whereas the compound nucleus is formed at a fixed relative separation ΔR (fixed ΔR). Also, we observe that all three forces SLy4, SkM*, and, KDE0(v1) behave nearly alike, except for the relative depths of their minima. Figure 9 presents the calculated evaporation channel cross sections as a function of angular momentum ℓ for the reaction $^{244}\text{Pu} + ^{48}\text{Ca}$ and shows an increase with ℓ up to about $49\hbar$ for SLy4 and $45\hbar$ for SkM*, and $50\hbar$ for KDE0(v1) forces, but then a decrease with the increase of ℓ . Here, we have fixed the maximum (ℓ_{max}) and minimum (ℓ_{min}) values of angular momentum for the calculated channel cross sections σ_{xn} for $x = 3-5$ which becomes

negligibly small ($\sigma_{xn} < 10^{-18}$ mb, $x = 3, 4$, and 5) for the ℓ values other than those lying in the range $\ell_{\text{min}} \leq \ell \leq \ell_{\text{max}}$. Thus, for the limiting value of $\sigma_{xn} < 10^{-18}$ mb, the window is set as $26\hbar \leq \ell \leq 70\hbar$, i.e., $\ell_{\text{max}} = 70\hbar$ and $\ell_{\text{min}} = 26\hbar$.

In Fig. 10, we have compared experimental and the DCM calculated σ_{xn} , $x = 3n, 4n$, and $5n$ from $^{292}\text{Fl}^*$ at a fixed $E^* = 46.9$ MeV for the entrance channel $^{244}\text{Pu} + ^{48}\text{Ca}$. The experimental data are taken from Refs. [24–27] and the calculations are made for the neck-length parameter ΔR obtained for the best fit to $3n$, $4n$, and $5n$ evaporation residue cross section from ^{292}Fl using the three Skyrme forces namely (a) SLy4, (b) SkM*, and (c) KDE0(v1), as plotted in Fig. 11. Here, the application of SLy4 at each excitation energy E^* results in the largest ΔR for $4n$ emission followed by $5n$ and $3n$ emission and SkM* and KDE0(v1) forces results in largest ΔR for $5n$ followed by $4n$ and $3n$ emission (see Table II) from the compound system $^{292}\text{Fl}^*$. In a nutshell, we can say that the $4n$ emission occurs the earliest, then $5n$ emission, in complete agreement with experimental data implies that compound system $^{288}\text{Fl}^*$ has the highest cross section and $^{287}\text{Fl}^*$ the lowest. Clearly, as shown in Table II, for all three forces, the $4n$ decay channel has the

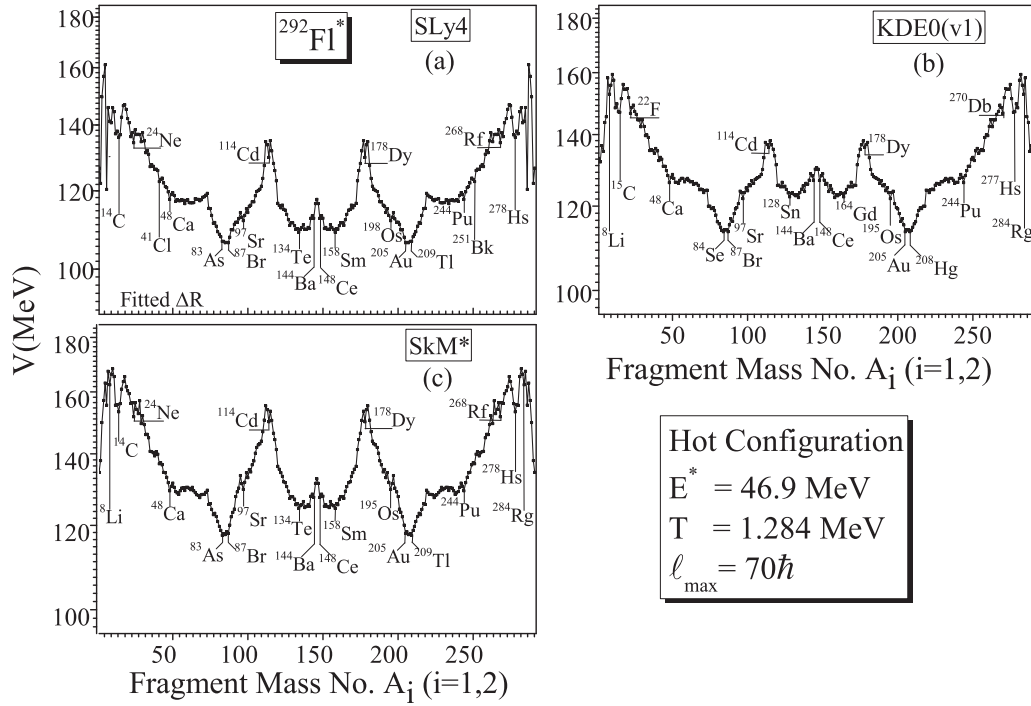


FIG. 8. Same as Fig. 3, but for $\Delta R_{3n,4n,5n} = 1.8262, 2.2056,$ and 2.1381 fm for SLy4 force; $\Delta R_{3n,4n,5n} = 1.8159, 2.2128,$ and 2.4696 fm for SkM* force and $\Delta R_{3n,4n,5n} = 1.7026, 1.9660,$ and 2.1786 fm for KDE0(v1) force which fits the data in Fig. 11 at $E^* = 46.9$ MeV for $3n, 4n,$ and $5n$ emission from $^{292}\text{Fl}^*$ formed via $^{244}\text{Pu} + ^{48}\text{Ca}$ reaction. The $\Delta R = 0.1$ fm is fixed for the light fragment masses $A_2 = 1-2$ and heavy fragment masses $A_2 = 6-143$.

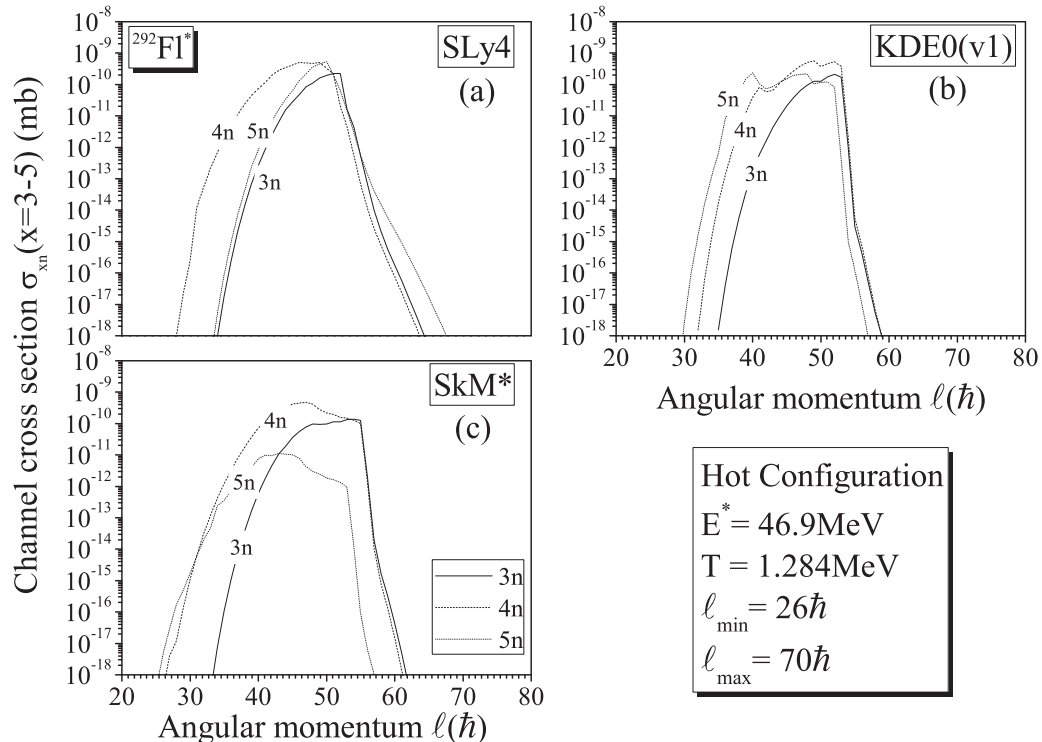


FIG. 9. Channel cross sections σ_{xn} , $x = 3, 4,$ and 5 , for $^{292}\text{Fl}^*$, plotted as a function of l , the cut-off point is $\sigma_{xn} < 10^{-18}$ mb, limiting $l_{\min} = 26\hbar, l_{\max} = 70\hbar$ for all three Skyrme forces.

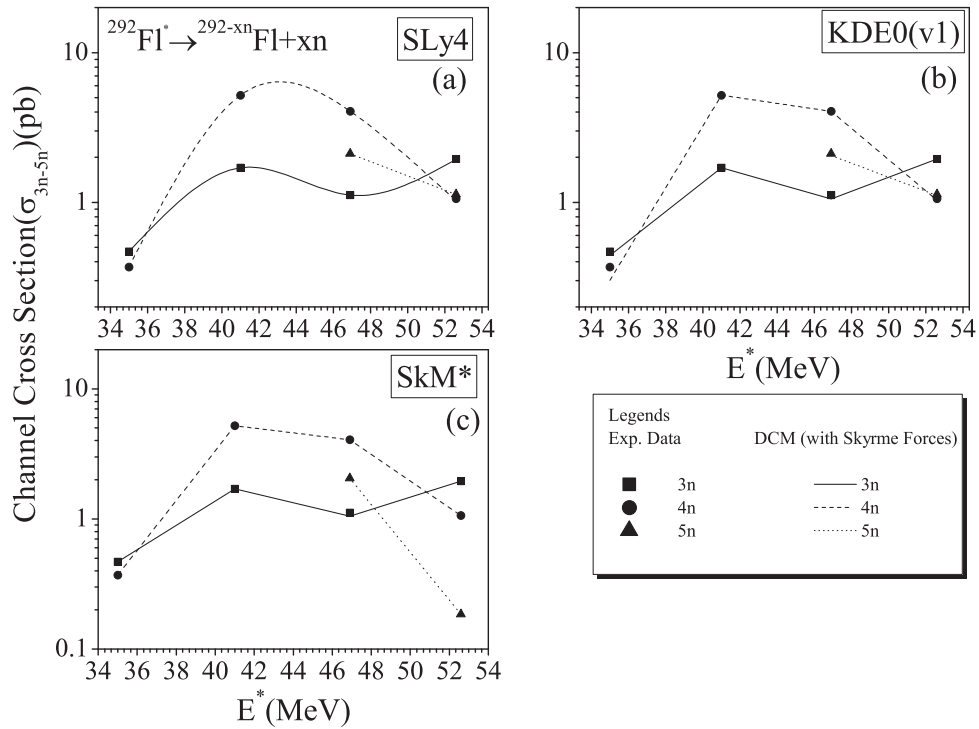


FIG. 10. Excitation function of $3n$, $4n$, and $5n$ evaporation channels for the $^{244}\text{Pu} + ^{48}\text{Ca}$ reaction in the “hot fusion” process. The experimental data (rectangle, circle, and triangle symbols) are from Refs. [24–27], and the solid, dashed, and dotted lines represent our calculations made for different Skyrme forces (a) SLy4, (b) SkM*, and (c) KDE0(v1) for the best fitted ΔR values given in Fig. 11. The calculations are made for the observed excitation energies E^* .

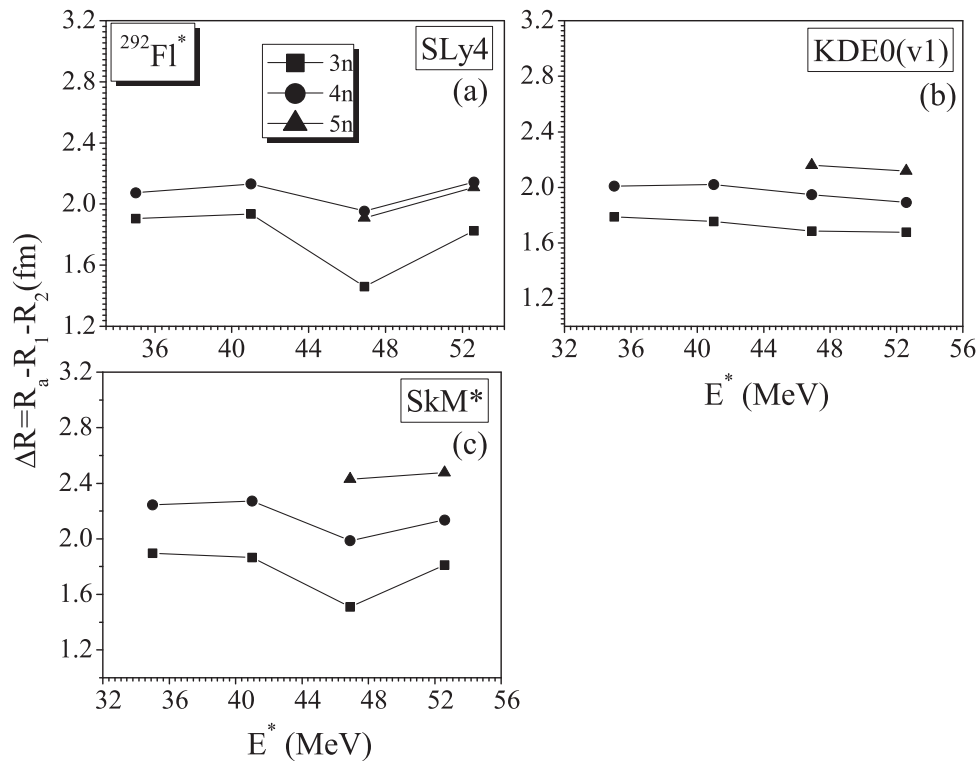


FIG. 11. The best fitted neck-length parameter ΔR as a function of excitation energy E^* for $3n$, $4n$, and $5n$ neutron ER from $^{292}\text{Fl}^*$ formed in the reaction channel $^{244}\text{Pu} + ^{48}\text{Ca}$ at an excitation energy of 35.0–52.6 MeV. The rectangle, circle, and triangle represent our calculations made for different Skyrme forces (a) SLy4, (b) SkM*, and (c) KDE0(v1), respectively.

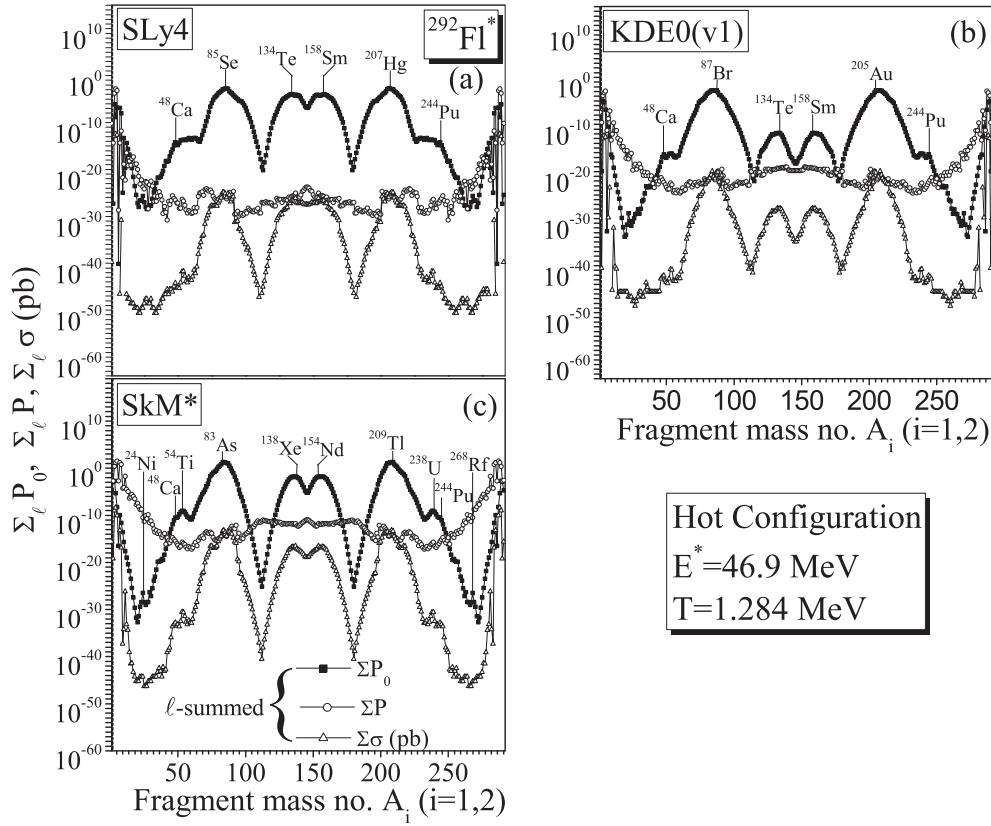


FIG. 12. ℓ -summed preformation probability P_0 , penetration probability P , and channel cross section σ_{A_i} , $i = 1, 2$, plotted as a function of fragment mass number A_i .

largest cross section, followed by $3n$ and $5n$ decay cross sections, in complete agreement with experimental results. Apparently, the DCM reproduces the data nicely within one parameter fitting ΔR , nearly independent of the Skyrme force used.

Figure 12 shows a plot of ℓ -summed penetration probability P , preformation probability P_0 , and channel cross section σ_{A_i} , plotted as a function of fragment mass number. We notice that, for all the three Skyrme forces, $P(A_i)$ is nearly constant and contributes only to the magnitude of the cross section, $P_0(A_i)$ provides the structure to the cross section. An interesting result of this graph is that CN $^{292}\text{Fl}^*$ decay via symmetric fission and the predicted fission mass region, say for all three forces, is 134 to 158 , i.e., $A/2 \pm 12$. Further the quasifission peaks appears at ^{207}Hg ($+ ^{85}\text{Se}$) for SLy4, at ^{209}Tl ($+ ^{83}\text{As}$) for SkM* and at ^{205}Au ($+ ^{87}\text{Br}$), similar to one observed experimentally in superheavy nucleus $Z = 122$ [72–74]. The predicted fission cross section ($\sigma_{ff}^{\text{predicted}}$) for CN $^{292}\text{Fl}^*$ at $E^* = 46.9$ MeV comes out to be 4.99×10^{-21} mb for the SLy4 force, 2.49×10^{-13} mb for the SkM* force, and 2.96×10^{-16} mb for the KDE0(v1) force. In Table III, we have also presented our calculations for the other proposed t-p combinations for “hot fusion” reactions at an illustrative $E^* = 49.6$ MeV, using the same neck length parameters as extracted from Fig. 12 and Table II for the $^{244}\text{Pu} + ^{48}\text{Ca}$ reaction. In addition, the calculated values of P_{CN} and P_{surv} are 0.698 and 0.881 at $E^* = 46.9$ MeV and are 0.999 and 0.790 at

TABLE III. The DCM predicted ER cross sections σ_{xn} for $3n$, $4n$, and $5n$ decay channels of $^{292}\text{Fl}^*$, formed in the $^{244}\text{Pu} + ^{48}\text{Ca}$ “hot fusion” reaction proposed on the basis of QMFT, at $E^* = 46.9$ MeV, for all three Skyrme forces.

$A_1 + A_2$	$\sigma_{3n}(\text{pb})$	$\sigma_{4n}(\text{pb})$	$\sigma_{5n}(\text{pb})$
For Skyrme force SLy4			
$^{284}\text{Rg} + ^8\text{Li}$	3.36×10^{-4}	9.31×10^{-5}	1.33×10^{-1}
$^{278}\text{Hs} + ^{14}\text{C}$	2.64×10^{-4}	1.42×10^{-5}	5.09×10^{-4}
$^{268}\text{Rf} + ^{24}\text{Ne}$	1.06×10^{-4}	9.80×10^{-6}	4.22×10^{-4}
$^{263}\text{Md} + ^{29}\text{Al}$	3.29×10^{-5}	6.05×10^{-6}	3.11×10^{-4}
$^{254}\text{Cf} + ^{38}\text{S}$	1.29×10^{-6}	6.92×10^{-7}	1.26×10^{-5}
$^{238}\text{U} + ^{54}\text{Ti}$	1.39×10^{-9}	5.22×10^{-9}	1.87×10^{-9}
For Skyrme force SkM*			
$^{284}\text{Rg} + ^8\text{Li}$	1.06×10^{-3}	4.3×10^{-3}	4.44×10^{-3}
$^{278}\text{Hs} + ^{14}\text{C}$	8.42×10^{-4}	2.39×10^{-4}	1.88×10^{-3}
$^{268}\text{Rf} + ^{24}\text{Ne}$	2.99×10^{-4}	9.28×10^{-5}	6.99×10^{-6}
$^{263}\text{Md} + ^{29}\text{Al}$	9.73×10^{-7}	2.93×10^{-5}	2.43×10^{-6}
$^{254}\text{Cf} + ^{38}\text{S}$	2.64×10^{-6}	1.4×10^{-6}	2.26×10^{-8}
$^{238}\text{U} + ^{54}\text{Ti}$	4.61×10^{-13}	6.6×10^{-12}	3.26×10^{-13}
For Skyrme force KDE0(v1)			
$^{284}\text{Rg} + ^8\text{Li}$	1.11×10^{-2}	7.76×10^{-2}	8.19×10^{-3}
$^{278}\text{Hs} + ^{14}\text{C}$	9.78×10^{-3}	9.13×10^{-2}	1.19×10^{-2}
$^{268}\text{Rf} + ^{24}\text{Ne}$	3.34×10^{-3}	4.27×10^{-2}	7.25×10^{-3}
$^{263}\text{Md} + ^{29}\text{Al}$	1.06×10^{-3}	1.79×10^{-2}	4.02×10^{-3}
$^{254}\text{Cf} + ^{38}\text{S}$	1.23×10^{-5}	2.18×10^{-4}	8.12×10^{-5}
$^{238}\text{U} + ^{54}\text{Ti}$	9.36×10^{-15}	1.78×10^{-13}	2.25×10^{-13}

TABLE IV. The excitation functions of $1n$, $2n$, $4n$, and $5n$ evaporation channels (experimentally unobserved) from $^{287,288,290,292}\text{Fl}^*$ due to entrance channels $^{239,240,242,244}\text{Pu} + ^{48}\text{Ca}$ predicted by using the DCM for a best fit of ΔR , at different $E^* = 32.5$ MeV to 52.6 MeV energies by using SkM* Skyrme force.

E^* (MeV)	xn	T (MeV)	$\sigma_{\text{predicted}}^{\text{DCM}}$ (pb)
$^{244}\text{Pu} + ^{48}\text{Ca}$			
35	$1n$	1.112	4.57×10^{-21}
35	$2n$	1.112	2.11×10^{-23}
35	$5n$	1.112	3.09×10^{-44}
41	$1n$	1.202	2.06×10^{-16}
41	$2n$	1.202	5.93×10^{-21}
41	$5n$	1.202	8.39×10^{-42}
46.9	$1n$	1.284	1.05×10^{-14}
46.9	$2n$	1.284	6.8×10^{-20}
52.6	$1n$	1.359	3.12×10^{-14}
52.6	$2n$	1.359	2.57×10^{-19}
$^{242}\text{Pu} + ^{48}\text{Ca}$			
32.5	$1n$	1.076	3.91×10^{-29}
32.5	$4n$	1.076	3.15×10^{-47}
32.5	$5n$	1.076	2.65×10^{-52}
35.3	$1n$	1.116	1.53×10^{-28}
35.3	$2n$	1.116	2.49×10^{-35}
35.3	$5n$	1.116	1.72×10^{-51}
40.2	$1n$	1.195	5.63×10^{-27}
40.2	$2n$	1.195	3.05×10^{-33}
40.2	$5n$	1.195	1.73×10^{-50}
$^{240}\text{Pu} + ^{48}\text{Ca}$			
38.6	$1n$	1.175	9.82×10^{-27}
38.6	$2n$	1.175	2.12×10^{-33}
38.6	$5n$	1.175	3.55×10^{-60}
$^{239}\text{Pu} + ^{48}\text{Ca}$			
37.6	$1n$	1.162	4.22×10^{-43}
37.6	$2n$	1.162	1.06×10^{-46}
37.6	$3n$	1.162	4.7×10^{-43}
35.3	$4n$	1.162	2.0×10^{-80}

$E^* = 52.6$ MeV. Here, we have seen that P_{CN} increases (equivalently, σ_{nCN} decreases) and P_{surv} decreases (equivalently, σ_{ff} increases) with an increase of E^* for both the reactions, in agreement with the experimental work [73,74].

IV. SUMMARY AND CONCLUSIONS

To summarize, the synthesis and decay of superheavy Fl isotopes are studied via the fusion-evaporation reaction mechanism within the DCM model including effects of quadrupole deformations and compact orientations. First of all, quantum mechanical fragmentation theory (QMFT) involving nuclear interaction potentials derived from SEDF based on the semi-classical ETF approach with densities added in the frozen densities approximation is used to identify the t-p combinations, referring to potential energy minima, for the formation of CN $^{287,288,290,292}\text{Fl}^*$ at a fixed relative separation ΔR (within a nuclear limit of ≈ 2 fm) at a given excitation energy

E^* . We take three Skyrme forces namely, SLy4, SkM*, and KDE0(v1) which account for the properties of both the normal and isospin-rich nuclei, with nuclei considered quadrupole deformed and optimally hot oriented, lying in the same plane (coplanar nuclei). An interesting result is that, in addition to a hot fusion reaction, namely $^{239,240,242,244}\text{Pu} + ^{48}\text{Ca}$ already used in experiments to synthesize $^{287,288,290,292}\text{Fl}^*$, a number of other reactions are predicted which are lying at minimum in PES, shown in Fig. 7 and Table I for Skyrme force SkM* along with their other characteristics, such as quadrupole deformations β_{2i} , calculated barrier heights V_B , and barrier positions R_B for optimum hot orientations. We have calculated channel cross sections for the predicted t-p combinations having hot-compact configuration since it favors symmetric fission, in complete agreement with experiments. Here, we suggest $^{42}\text{Ar} + ^{245,246,248}\text{Cm}$ and $^{238}\text{U} + ^{54}\text{Ti}$ for the synthesis of CN $^{287,288,290}\text{Fl}^*$ and $^{292}\text{Fl}^*$, respectively, in future experiments. It is well known that the combination of stable projectiles with actinide targets is a good way to produce neutron-deficient SHN. While a number of neutron-rich SHN cannot be obtained in this way, the use of radioactive beams may provide a possibility in the formation of several neutron-rich nuclei. The use of radioactive beams may provide a possibility only if the intensity of the radioactive beams were improved to an extremely high quantity or some specific detection devices were to be found. In terms of the current experimental setup, the use of radioactive ion beams is not a promising method to produce neutron-rich SHN [75].

The Skyrme force included DCM is used to calculate the fusion excitation function of optimum hot fusion reactions $^{239,240,242,244}\text{Pu} + ^{48}\text{Ca}$, giving a nice description of data, independent of the Skyrme force used, within one parameter fitting of neck-length (ΔR). From Table II, we can see that the evaporation residue cross section of producing SHN depends on the neutron to proton ratio of the target and projectile in hot fusion reactions. In our case, we have fixed the projectile and for different targets and have calculated the evaporation residue cross section. For example, the maximal evaporation residue cross section is 2.6 pb for the reaction $^{240}\text{Pu}(^{48}\text{Ca}, 4n)^{287}\text{Fl}$. However, using two more neutron isotopes as the target $^{242}\text{Pu}(^{48}\text{Ca}, 4n)^{288}\text{Fl}$, the experimental evaporation residue cross section was enhanced from 2.6 pb to 4.5 pb. And then further by using two more neutron isotopes as the target $^{244}\text{Pu}(^{48}\text{Ca}, 4n)^{290}\text{Fl}$, the experimental evaporation residue cross section for producing $Z = 114$ increased from 4.5 pb to 5.19 pb. Our calculation also reproduced the same tendency. Therefore, a target with a larger number of neutrons is expected to increase the evaporation residue cross section of SHN.

We have also calculated evaporation residue cross sections for experimentally unobserved $1n$, $2n$, and $4n$ channels at different $E^* = 32.5$ MeV to 52.6 MeV by using the SkM* Skyrme force and corresponding data shown in Table IV. The predicted fission mass region lies at $A = 134$ to $A = 158$, i.e., $A/2 \pm 12$, and the quasifission peaks appears at $^{206}\text{Hg}(+^{86}\text{Se})$ for SLy4, at $^{209}\text{Tl}(+^{83}\text{As})$ for SkM*, and at $^{205}\text{Au}(+^{87}\text{Br})$ for KDE0(v1) Skyrme force. Here, it is important to note that despite a dominating contribution of the quasifission process for the reaction in the symmetric region of fission fragment

masses ($A/2 \pm 20$), the process of the fusion-fission of CN prevails and it agrees well with experimental works [23,74]. The predicted fission cross sections ($\sigma_{ff}^{\text{predicted}}$) for CN $^{292}\text{Fl}^*$ at $E^* = 46.9$ MeV for all three forces are calculated and further used to calculate P_{CN} and P_{surv} . We have observed the variation of the magnitude of P_{CN} and P_{surv} with excitation energies E^* and have found that the dominant factor in the variation of the product $P_{\text{CN}}P_{\text{surv}}$ is P_{surv} .

ACKNOWLEDGMENTS

We are very grateful to late Emeritus Prof. Raj K. Gupta, Department of Physics, Panjab University, Chandigarh for his fruitful guidance and support to this work. One of the authors (N.K.) would like to thank University Grants Commission for financial support under reference no. 1294/(CSIR-UGC NET JUNE 2017).

-
- [1] J. Hong *et al.*, *Phys. Lett. B* **809**, 135760 (2020).
- [2] C. W. Shen, Y. Abe, D. Boilley, G. Kosenko, and E. G. Zhao, *Int. J. Mod. Phys. E* **17**, 66 (2008).
- [3] Z. H. Liu and J. D. Bao, *Phys. Rev. C* **80**, 054608 (2009).
- [4] V. I. Zagrebaev, *Phys. Rev. C* **64**, 034606 (2001).
- [5] J. Sadhukhan, W. Nazarewicz, and N. Schunck, *Phys. Rev. C* **93**, 011304(R) (2016).
- [6] H. Eslamizadeh, *Phys. Rev. C* **104**, 034601 (2021).
- [7] B. Schuetrumpf and W. Nazarewicz, *Phys. Rev. C* **96**, 064608 (2017).
- [8] T. Nakatsukasa, K. Matsuyanagi, M. Matsuo, and K. Yabana, *Rev. Mod. Phys.* **88**, 045004 (2016).
- [9] A. S. Umar and V. E. Oberacker, *Nucl. Phys. A* **944**, 238 (2015).
- [10] L. Q. Li, G. Zhang, and F. S. Zhang, *Phys. Rev. C* **106**, 024601 (2022).
- [11] G. Zhang, C. Li, P.W. Wen, J.J. Li, X.X. Xu, B. Li, Z. Liu, and F.S. Zhang, *Phys. Rev. C* **98**, 014613 (2018).
- [12] R. K. Gupta, M. Balasubramaniam, R. Kumar, D. Singh, C. Beck, and W. Greiner, *Phys. Rev. C* **71**, 014601 (2005).
- [13] R. K. Gupta, M. Manhas, and W. Greiner, *Phys. Rev. C* **73**, 054307 (2006).
- [14] N. Kumari, A. Deep, and R. Kharab, *Phys. Rev. C* **105**, 014628 (2022).
- [15] R. Eichler *et al.*, *Radiochim. Acta* **98**, 133 (2010).
- [16] C. S. Nash, *J. Phys. Chem. A* **109**, 3493 (2005).
- [17] D. C. Hoffman *et al.*, *The Chemistry of the Actinide and Transactinide Elements*, 3rd ed. (Springer, Berlin, 2006), pp. 1652–1752.
- [18] A. Yakushev *et al.*, *Inorg. Chem.* **53**, 1624 (2014).
- [19] J. X. Li, W. X. Wang, and H. F. Zhang, *Phys. Rev. C* **106**, 044601 (2022).
- [20] R. K. Gupta *et al.*, *Int. J. Mod. Phys. E* **18**, 601 (2009).
- [21] J. Blocki, J. Randrup, W. J. Swiatecki, and C. F. Tsang, *Ann. Phys. (NY)* **105**, 427 (1977).
- [22] M. Kaur, R. Kumar, and M. K. Sharma, *Phys. Rev. C* **85**, 014609 (2012).
- [23] M. G. Itkis *et al.*, *J. Nucl. Radiochem. Sci.* **3**, 57 (2002).
- [24] Yu. Ts. Oganessian *et al.*, *Phys. Rev. C* **70**, 064609 (2004).
- [25] Yu. Ts. Oganessian *et al.*, *Phys. Rev. C* **69**, 054607 (2004).
- [26] V. K. Utyonkov *et al.*, *Phys. Rev. C* **92**, 034609 (2015).
- [27] V. K. Utyonkov *et al.*, *Phys. Rev. C* **97**, 014320 (2018).
- [28] X. J. Bao, S. Q. Guo, H. F. Zhang, and J. Q. Li, *Phys. Rev. C* **96**, 024610 (2017).
- [29] J. Li, C. Li, G. Zhang, B. Li, X. Xu, Z. Liu, Y. S. Tsyganov, and F. S. Zhang, *Phys. Rev. C* **98**, 014626 (2018).
- [30] S. Chopra, A. Kaur, Hemdeep, and R. K. Gupta, *Phys. Rev. C* **93**, 044604 (2016).
- [31] R. K. Gupta, D. Singh, R. Kumar, and W. Greiner, *J. Phys. G: Nucl. Part. Phys.* **36**, 075104 (2009).
- [32] R. K. Gupta, A. Săndulescu, and W. Greiner, *Phys. Lett. B* **67**, 257 (1977).
- [33] J. Maruhn and W. Greiner, *Phys. Rev. Lett.* **32**, 548 (1974).
- [34] R. K. Gupta, W. Scheid, and W. Greiner, *Phys. Rev. Lett.* **35**, 353 (1975).
- [35] A. Săndulescu, R. K. Gupta, W. Scheid, and W. Greiner, *Phys. Lett. B* **60**, 225 (1976).
- [36] R. K. Gupta, *Sov. J. Part. Nucl.* **8**, 289 (1977).
- [37] A. Deep, Niyti, R. Kharab, R. Singh, and S. Chopra, *Phys. Rev. C* **102**, 034607 (2020).
- [38] A. Deep, Niyti, R. Kharab, R. Singh, and S. Chopra, *Int. J. Mod. Phys. E* **28**, 1950079 (2019).
- [39] R. K. Gupta, M. Balasubramaniam, C. Mazzocchi, M. La Commara, and W. Scheid, *Phys. Rev. C* **65**, 024601 (2002).
- [40] R. K. Gupta, R. Kumar, N. K. Dhiman, M. Balasubramaniam, W. Scheid, and C. Beck, *Phys. Rev. C* **68**, 014610 (2003).
- [41] M. Balasubramaniam, R. Kumar, R. K. Gupta, C. Beck, and W. Scheid, *J. Phys. G: Nucl. Part. Phys.* **29**, 2703 (2003).
- [42] R. K. Gupta, M. Balasubramaniam, R. Kumar, N. Singh, M. Manhas, and W. Greiner, *J. Phys. G: Nucl. Part. Phys.* **31**, 631 (2005).
- [43] R. K. Gupta, M. Balasubramaniam, R. Kumar, D. Singh, S. K. Arun, and W. Greiner, *J. Phys. G: Nucl. Part. Phys.* **32**, 345 (2006).
- [44] R. K. Gupta, S. K. Arun, R. Kumar, and Niyti, *Int. Rev. Phys. (IREPHY)* **2**, 369 (2008).
- [45] B. B. Singh, M. K. Sharma, and R. K. Gupta, *Phys. Rev. C* **77**, 054613 (2008).
- [46] S. K. Arun, R. Kumar, and R. K. Gupta, *J. Phys. G: Nucl. Part. Phys.* **36**, 085105 (2009).
- [47] R. Kumar and R. K. Gupta, *Phys. Rev. C* **79**, 034602 (2009).
- [48] R. Kumar, M. Bansal, S. K. Arun, and R. K. Gupta, *Phys. Rev. C* **80**, 034618 (2009).
- [49] R. K. Gupta, in *Lecture Notes in Physics 818, Clusters in Nuclei*, edited by C. Beck (Springer-Verlag, Berlin, 2010), Vol. I, p. 223.
- [50] M. K. Sharma, G. Sawhney, R. K. Gupta, and W. Greiner, *J. Phys. G: Nucl. Part. Phys.* **38**, 105101 (2011).
- [51] M. K. Sharma, S. Kanwar, G. Sawhney, and R. K. Gupta, *Phys. Rev. C* **85**, 064602 (2012).
- [52] M. Bansal, S. Sahila, R. K. Gupta, R. Kumar, and M. K. Sharma, *Phys. Rev. C* **86**, 034604 (2012).
- [53] S. Chopra, M. Bansal, M. K. Sharma, and R. K. Gupta, *Phys. Rev. C* **88**, 014615 (2013).
- [54] H. Kröger and W. Scheid, *J. Phys. G* **6**, L85 (1980).
- [55] R. K. Gupta, in *Nuclear Particle Correlations and cluster Physics*, edited by W. U. Schröder (World Scientific Publishers, Singapore, 2017), Chap. 18.

- [56] S. Kumar and R. K. Gupta, *Phys. Rev. C* **55**, 218 (1997).
- [57] T. Matsuse, C. Beck, R. Nouicer, and D. Mahboub, *Phys. Rev. C* **55**, 1380 (1997).
- [58] S. J. Sanders, D. G. Kovar, B. B. Back, C. Beck, D. J. Henderson, R. V. F. Janssens, T. F. Wang, and B. D. Wilkins, *Phys. Rev. C* **40**, 2091 (1989).
- [59] S. J. Sanders, *Phys. Rev. C* **44**, 2676 (1991).
- [60] N. J. Davidson, S. S. Hsiao, J. Markram, H. G. Miller, and Y. Tzeng, *Nucl. Phys. A* **570**, 61c (1994).
- [61] G. Audi, A. H. Wapstra, and C. Thibault, *Nucl. Phys. A* **729**, 337 (2003).
- [62] W. Myers and W. J. Swiatecki, *Nucl. Phys.* **81**, 1 (1966).
- [63] P. Möller, J. R. Nix, W. D. Myers, and W. J. Swiatecki, *At. Data Nucl. Data Tables* **59**, 185 (1995).
- [64] R. Kumar, M. K. Sharma, and R. K. Gupta, *Nucl. Phys. A* **870–871**, 42 (2011).
- [65] Niyti, A. Deep, R. Kharab, S. Chopra, and R. K. Gupta, *Phys. Rev. C* **95**, 034602 (2017).
- [66] B. K. Agrawal, S. K. Dhiman, and R. Kumar, *Phys. Rev. C* **73**, 034319 (2006).
- [67] D. Vautherin and D. M. Brink, *Phys. Rev. C* **5**, 626 (1972).
- [68] M. Brack, C. Guet, and H.-B. Hakansson, *Phys. Rep.* **123**, 275 (1985).
- [69] B. K. Agrawal, S. Shlomo, and V. K. Au, *Phys. Rev. C* **72**, 014310 (2005).
- [70] J. Bartel and K. Bencheikh, *Eur. Phys. J. A* **14**, 179 (2002).
- [71] G.-Q. Li, *J. Phys. G: Nucl. Part. Phys.* **17**, 1127 (1991).
- [72] M. G. Itkis *et al.*, *Nucl. Phys. A* **734**, 136 (2004).
- [73] E. M. Kozulin *et al.*, *Phys. Rev. C* **90**, 054608 (2014).
- [74] E. M. Kozulin *et al.*, *Phys. Rev. C* **99**, 014616 (2019).
- [75] Z. H. Wu, L. Zhu, F. Li, X. B. Yu, J. Su, and C. C. Guo, *Phys. Rev. C* **97**, 064609 (2018).